Research Article

Effect of Over Zone Feeding on Rail Potential and Stray Current in DC Mass Transit System

Guifu Du, Chonglin Wang, Jianhua Liu, Guoxin Li, and Dongliang Zhang

School of Information and Electrical Engineering, China University of Mining and Technology, Xuzhou 221008, China

Correspondence should be addressed to Jianhua Liu; ljh5605@126.com

DC traction power system with running rails as reflux conductor has been adopted in Guangzhou Metro Line 8. During the operation of the Guangzhou Metro Line, a high rail potential has been observed, and the leakage of stray current increases significantly. Because of the electrical connectivity of the catenary, over zone feeding of traction current may exist when multiple trains run in multiple traction substations. Guangzhou Metro Line 8 suspects that over zone feeding of traction current is the major cause of the high rail potential. In this paper, a unified chain model of DC traction power system is proposed to simulate the distribution of rail potential and stray current. Field tests and simulations have been carried out to study whether over zone feeding has an impact on rail potential and stray current. Results show that over zone feeding widely exists in DC traction power system and that the rail potential and stray current can be reduced effectively by preventing the over zone feeding of traction current.

1. Introduction

In 1500 V DC traction power system of Guangzhou Metro Line 8, the train obtains power from the catenary, and the running rails are used as return conductor for traction current. Ungrounded scheme of the negative return conductor with over voltage protection device (OVPD) is adopted in the line. There will be a potential between the running rails and the ground, known as rail potential, which is caused by the resistance of running rails and traction current transmission [1–3]. A high rail potential may cause damage to human safety, and it will increase the leakage of return current at the same level of rail-to-ground insulation, known as stray current. Then, electrochemical corrosion will be exacerbated [4]. A high rail potential, up to 90 V or higher, has been observed during the operation of DC mass transit system in multiple lines of Guangzhou Metro [5]. OVPD is adopted in order to control rail potential by connecting the running rails to the substation ground [2]. However, it is activated frequently, up to hundreds of times, during the operation of Guangzhou Metro Line. Some OVPDs are turned on and keep the running rails grounded, in which case the current leakage from the OVPD can reach 800 A [6]. It is a great threat to the operational safety of the line and the protection of stray current.

The causes and control methods have been researched on rail potential and stray current by some scholars. Relative researches show that [3, 7, 8], by reducing the resistance of the running rail, increasing the voltage level of traction power system, and shortening the distance between substations, the rail potential and stray current can be reduced. Furthermore, different grounding schemes of the DC mass transit system, including ungrounded, solidly grounded, and diode-grounded, have an influence on the rail potential and stray current [2, 3, 9]. In Taipei rapid transit systems, the impedance bond between Blue and Red-Green line is proved to be a cause of high rail potential and stray current [10, 11]. Moreover, the researches show that running modes of train have an impact on rail potential and stray current [12]. Rail potential is relatively high during acceleration and brake of the train and the maximum rail potential occurs at the position of the train. Simulation model of rail potential and stray current has been studied in many researches. In lumped parameter model of rail potential and stray current [1, 10, 13], a segment of 100 m is sufficient and accurate for the simulation, but the conductance matrixes of multiple zones

will be very large, and the speed of calculation will be slow. In distributed parameter model of rail potential and stray current [3, 9, 12], traction current of each node is obtained from flow calculation of DC traction power system. The accuracy of power flow calculation depends on the precise modification of the reflux system parameter. Nevertheless, the flow calculation and the evaluation of rail potential are not combined with each other. In order that more factors can be considered in assessment of rail potential and stray current, new simulation models have been proposed by scholars. Rail potential and stray current are modeled by a finite element method in [14], and the introduction of an equipotential connection between the reinforcement bars of the adjacent segments is proposed to prevent corrosion phenomena. A commercial software platform (CDEGS) can be used in assessing the more complex stray current with the effect of crosstrack regeneration supply [15]. With the same platform, a topologically accurate model in cut-and-cover sections of DC metro systems is presented to evaluate the dynamic stray current picture [16]. In [17], the factors, such as the train characteristics, time tabling, headway, and multiple trains' movement, are considered in the assessment of rail potential and stray current.

In view of above contributions, the work presented in this paper reinforces the effect of over zone feeding on rail potential and stray current. The regenerative power fed back to the catenary from braking train may be consumed by trains running in other zones owing to the electrical connectivity of the catenary and unilateral conductivity of the 24-pulse rectifier units [18, 19]. Distribution of the regenerative power is related to the powers and positions of other trains and the regenerative energy absorbing device. In this paper, the effect of over zone feeding on rail potential and stray current is tested in Guangzhou Metro Line 8. A multiconductor model of DC traction power system is established based on the actual features of the system. For the realization of fast and accurate calculation, lumped parameters of reflux system in the model are modified based on lumped parameter model and distributed parameter model. A chain model of DC traction power system is proposed to unify the complicated operation modes of traction substation and train. Rail potential and stray current affected by over zone feeding can be analyzed by the simulation model.

2. System Description

Field tests of over zone feeding on rail potential have been carried out in Guangzhou Metro Line 8. The total length of Guangzhou Metro Line 8 is 18.48 km. It includes 7 traction substations and 6 train stations. Configuration of Guangzhou Metro Line 8 is shown in Figure 1.

The high-voltage system for Guangzhou Metro Line 8 is 110 kV. It is stepped down to 33 kV by the Bulk Supply Substation. Then the 33 kV is supplied for the rectifier units and the train substation. No-load voltage of the rectifier units is 1593 V, which is distributed to the catenaries of the up-line and down-line. Traction current of the train comes from the catenary and returns to the negative bus of the rectifier units
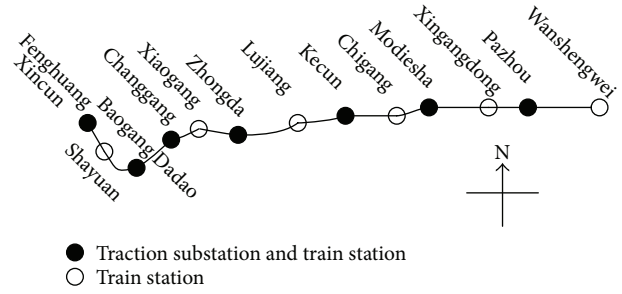

FIGURE 1: Configuration of Guangzhou Metro Line 8.

by running rails and negative return cable. Schematic of DC mass transit system is shown in Figure 2.

A 24-pulse diode transformer rectifier is widely used in DC mass transit system to reduce harmonic components. Insulated joints are set between catenaries of adjacent power supply zones to ensure the power supplying safely, reliably, and flexibly. DC circuit-breakers B1~B4 connect the positive bus of the rectifier units to the catenaries on both sides of the insulated joint. The presence of DC bus and circuit-breakers leads to the electrical continuity of catenaries; therefore, all traction substations can supply power for multiple trains. Up-line rail and down-line rail are connected by cross-bonding cables at intervals of 400 m~500 m. Buried conductors are set in the ballast bed to collect stray current. Most traction current flows back to the negative bus of rectifier units through the running rails and the rest of it flows from the buried conductor or ground.

Power distribution is affected by the characteristics of traction substation and train. External characteristic of traction substation is influenced by impedance parameters of rectifier unit, impedance voltage of rectifier transformer, connection modes of rectifier, and so forth [19]. In this paper, output characteristic of the rectifier unit is simplified to line I in Figure 3(a). Line II indicates that the catenary voltage at traction substation is higher than the no-load voltage U_0, and the traction substation is out of operation.

A train's running mode in one zone is actually divided into three stages: acceleration, which requires high traction current; coasting, which requires low traction current; deceleration, which may require regenerative braking and feed the current back to catenary. The position and power of train running in line can be obtained by train movement calculation. A typical curve of traction power when one train runs in a zone of 1.2 km is shown in Figure 3(b). The regenerative energy of train is partly consumed by the train, the left of which is fed back to the catenary and causes the catenary voltage rise for the unilateral conductivity of rectifier units. Energy absorbing device is usually set at the traction substation or train to absorb regenerative energy and limit the catenary voltage in the presence of train regenerative braking. It will be activated to maintain the catenary voltage when the voltage reaches the limited point U_{lim}. Consistent with Guangzhou Metro Line 8, regenerative energy absorbing device is set on the train in the simulation model.
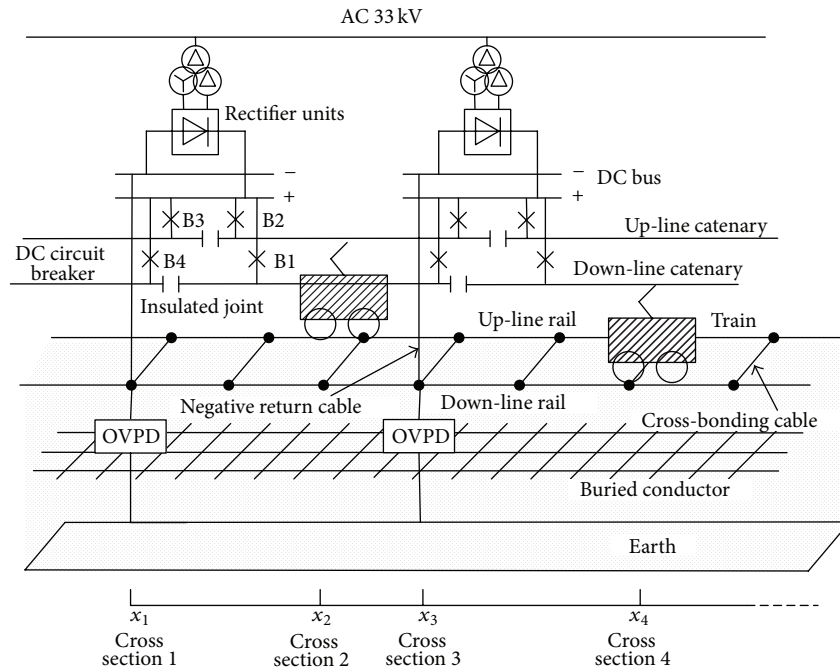
FIGURE 2: Schematic of DC mass transit system.

(a) Output characteristic of traction substation

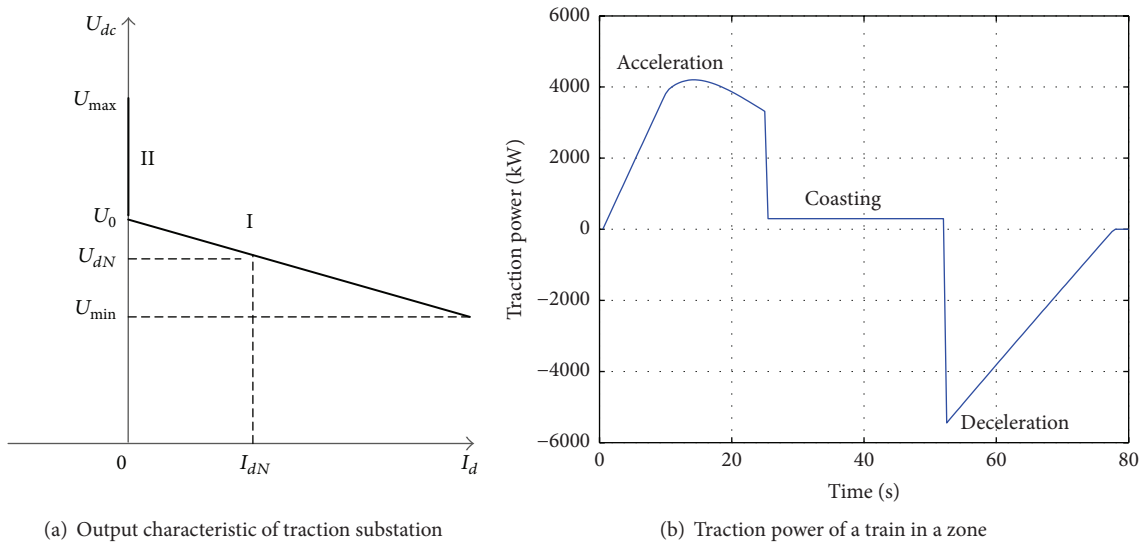(b) Traction power of a train in a zone

FIGURE 3: Characteristic of traction substation and train.

As shown in Figure 4, OVPD is installed in the substation to monitor the voltage between rail and local earth continuously for personal safety. The device will be activated if the measured voltage exceeds a preset voltage-time characteristic. Operating characteristic of the OVPD in Guangzhou Metro Line 8 is shown in Table 1.

3. Field Tests and Results

Field tests have been carried out at Wanshengwei Station and Pazhou Station in Guangzhou Metro Line 8 to assess the effect of over zone feeding on rail potential. Since Wanshengwei

Station is a train station without rectifier units, variation of traction current is relatively clear in single-side feeding zone from Pazhou Station to Wanshengwei Station. The distance between Wanshengwei Station and Pazhou Station is 1.8 km.

3.1. Field Tests of Traction Current. Connection modes of DC circuit-breakers B1~B4 are shown in Figure 2. Positive value of traction current in DC circuit-breakers is running from positive bus of the rectifier units to the catenary. Field tests have been carried out in Pazhou Station.

Traction currents in B1~B4 of Pazhou Station are shown in Figure 5 when a train Tr1 starts from Wanshengwei Station
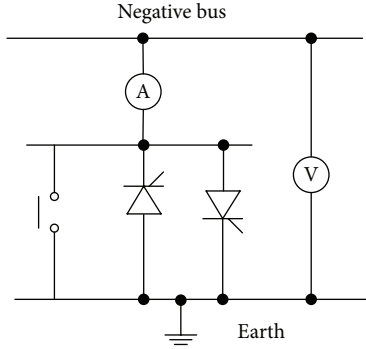
FIGURE 4: Schematic of the OVPD.

TABLE 1: Operating characteristic of the OVPD.

Symbol	Values	Operating characteristic
$U>$	92 VDC	Switches on with 0.1 s delay and switches off after 10 s.
$U\gg$	150 VDC	Switches on with no delay and switches off after 10 s.
$U\ggg$	600 VDC	Switches on with no delay and remains on until being switched off artificially

TABLE 2: Proportion of traction current coming from over zone feeding during Tr1 accelerates.

Time (s)	13.4	17.1	20.8	24.3	51.3
Traction current (A)	3048	2936	3216	3264	3725
CTR (%)	36.6	37.0	35.0	35.3	36.6

FIGURE 5: Traction current of Pazhou Substation.
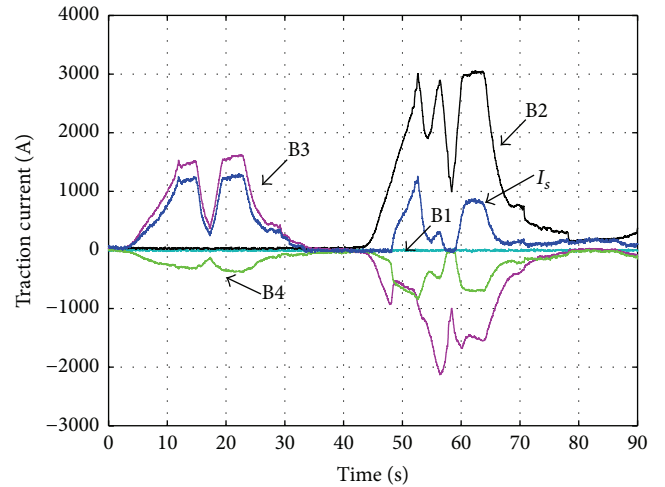
FIGURE 6: Traction current of Pazhou Station.

to Pazhou Station in up-line from 06:23:40 to 06:25:10 in December 21, 2012.

Since the zone is single-side feeding, all traction current of Tr1 flows from B2. Tr1 accelerates from Wanshengwei Station during 0.0 s~55.0 s, in which period current flowing from B2 is positive. The currents flowing from B3 and B4 are negative. At this moment, there is no regenerative braking train in line and the currents flowing from B3 and B4 are traction current provided by other substations. Traction current of Tr1 provided by Pazhou Station is shown as I_s in Figure 5, and currents flowing from B3 and B4 come from over zone feeding.

CTR is defined to describe the proportion of traction current coming from over zone feeding. We describe it as

$$\mathrm{CTR} = \left(\frac{I_{ct}}{I_t}\right) \times 100\%, \tag{1}$$

where I_{ct} is the traction current provided by other traction substations except substations in the zone of train running and I_t is traction current of the train.

Table 2 shows the CTR when traction current of Tr1 is high. Referring to Table 2 and Figure 5, proportions of traction current coming from over zone feeding are low and relatively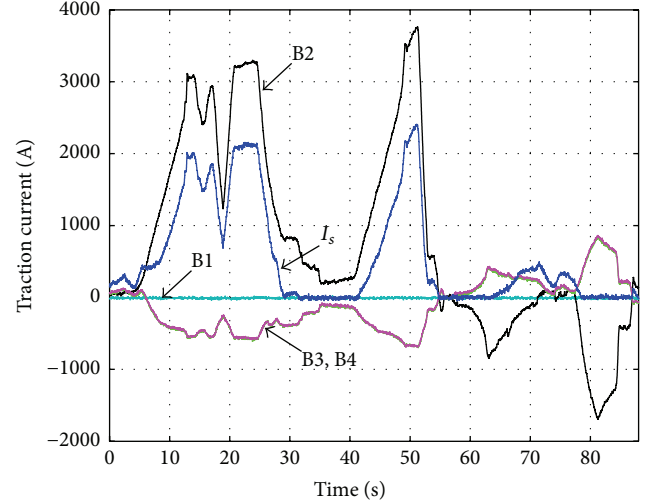 stable during 0.0 s~55.0 s. Current coming from over zone feeding is mainly provided by traction substations other than Pazhou Station.

Figure 6 shows traction currents in B1~B4 of Pazhou Station from 08:10:35 to 08:12:05 in December 21, 2012.

Traction currents in B1~B4 of Pazhou Station are shown in Figure 6. A train Tr2 accelerates from Pazhou Station to Xingangdong Station in up-line during 0.0 s~33.0 s. In this period, traction currents of B1 and B2 are 0.0 A for there is no train running in the single-side feeding zone. Tr3 accelerates from Wanshengwei Station to Pazhou Station at 43.0 s, and it absorbs energy from the catenary. At the same time, Tr2 begins regenerative braking and feeds energy back to the catenary. Then the regenerative current of Tr2 is fed to Tr3 over the zone. Current flowing from B3 is much higher than that shown in Figure 5 in this period.

Traction current provided by Pazhou Substation is shown as I_s in Figure 6. Traction current coming from over zone feeding increases greatly for there is an accelerating train Tr3 nearby the regenerative braking train Tr2. Table 3 shows

Table 3: Proportion of traction current coming from over zone feeding during Tr3 accelerates.

Time (s)	52.7	56.3	60.8	63.5	63.6
Traction current (A)	2989	2873	2981	3047	3033
CTR (%)	59.2	89.3	73.6	72.4	73.5

the CTR when traction current of Tr3 is high. With the same amplitude of train current, the CTR is much higher than that in Table 2. CTR reaches 89.3% at 56.3 s when the traction current of Tr3 is 2873 A.

Field tests of traction current show that over zone feeding exists widely in DC mass transit system for the electrical connectivity of the catenary. The extent of over zone feeding is related to various factors, including the density of trains in line, the power of trains, and the distance of traction substations. Traction current coming from over zone feeding will be large when the density of trains is high and the accelerating train is in a high coincidence with the regenerative braking train.

3.2. Field Tests of Rail Potential. Field tests of rail potential affected by over zone feeding have been carried out at Wanshengwei Station; at the same time, traction currents in B1~B4 of Pazhou Station are recorded. OVPD at Wanshengwei Station is activated frequently during the operation of the line.

As shown in Figure 7, parameters have been tested in three processes when train accelerates from Wanshengwei Station to Pazhou Station in up-line. The parameters include tractions current in B1~B4 of Pazhou Station, proportion of train current coming from over zone feeding, and rail potential at Wanshengwei Station.

In Figures 7(a)~7(c), traction current of the accelerating train is shown as B2, and there is little difference in the maximum amplitude of B2. However, the OVPD at Wanshengwei Station is activated at different moments of the accelerating processes.

As shown in Figure 7(a), there is no regenerative braking train nearby the accelerating Tr4. Therefore, traction current of Tr4 coming from over zone feeding is low and stable, which is provided by traction substations other than Pazhou Station. In this process, the rail potential is low and the OVPD is not activated.

Parameters are shown in Figure 7(b) during the acceleration of Tr5. From 0.0 s to 2.6 s, a large proportion of traction current comes from over zone feeding, while the amplitude of traction current coming from over zone feeding is low. Therefore, rail potential increases gradually but does not reach the limit $U >$ of OVPD. Traction current of Tr5 reaches the maximum from 7.2 s to 10.7 s and remains stable during this period. Nevertheless, the traction current coming from over zone feeding increases continuously. The rail potential of Wanshengwei Station reaches the limit $U >$ and OVPD is activated at the time 9.3 s. After 10.0 s, OVPD switches off.

Figure 7(c) shows the parameters during the acceleration of Tr6. Proportion of train current coming from over zone feeding is low and stable from the time 0.0 s to 12.0 s. During 12.0 s~13.8 s, traction current of Tr6 is low, and CTR increases rapidly to 100% for there is a train Tr7 regenerative braking in the zone of Pazhou Station to Xingangdong Station. From 14.5 s to 16.2 s, CTR decreases while amplitude of traction current coming from over zone feeding is increasing. Traction current amplitude of Tr6 reaches the maximum at 16.2 s, while the amplitude of traction current coming from over zone feeding is increasing continuously. The rail potential of Wanshegwei Station reaches the limit $U >$ and OVPD is activated at 16.7 s and it switches off after 10.0 s.

Results of field tests show that, in the same acceleration process, disparity exists in rail potential with different extent of over zone feeding. However, it is difficult to carry out the tests of real-time positions and currents of trains. A dynamic model is proposed to analyze the rail potential and stray current affected by over zone feeding in this paper.

4. Modeling of Rail Potential and Stray Current

Rail potential and stray current are associated with the distribution of power in DC traction power system. In this paper, a computational method of rail potential and stray current is proposed, which consists of two steps. Firstly, a chain model equivalent to the lumped parameter model of the system is proposed to carry out the power flow of the system. Secondly, rail potential and stray current are calculated by distributed parameter model of the reflux system, and the boundary conditions are obtained from power flow.

DC traction power system shown in Figure 2 can be expressed as the equivalent model shown in Figure 8. The catenary, traction substation, and train are lumped parameters, and the rail, buried conductor, and earth are distributed parameters. The up-line and down-line catenaries are independent in the interval and are connected by the DC positive bus at each traction substation. Output characteristic of the rectifier units is shown in Figure 3(a). The train is equivalent to a constant power model at each movement in the up-line, as P_2, or in down-line, as P_4 shown in Figure 8. The power and position of the train can be obtained from train movement calculation. P_{2r} or P_{4r} is energy absorbing device set on the train, which can be equivalent to a variable resistor. Due to the cross-bonds in the interval, the rails in up-line and down-line are equivalent to one conductor.

The mathematical problem can be described as follows: the model includes lumped parameters (catenary, traction substation, and train) and distributed parameters (rail, buried conductor, and earth). The location and external characteristics of each traction substation are predetermined. There are multiple trains running dynamically in up-line or down-line, which are modeled as constant power source in each movement. The power changing with time $p(t)$ and the position changing with time $x(t)$ of each train can be obtained by train movement calculation. In the model, the rail potential at each position changing with time $u_r(x, t)$, the potential of buried conductor at each position changing with time $u_s(x, t)$, the current in rail at each position changing with
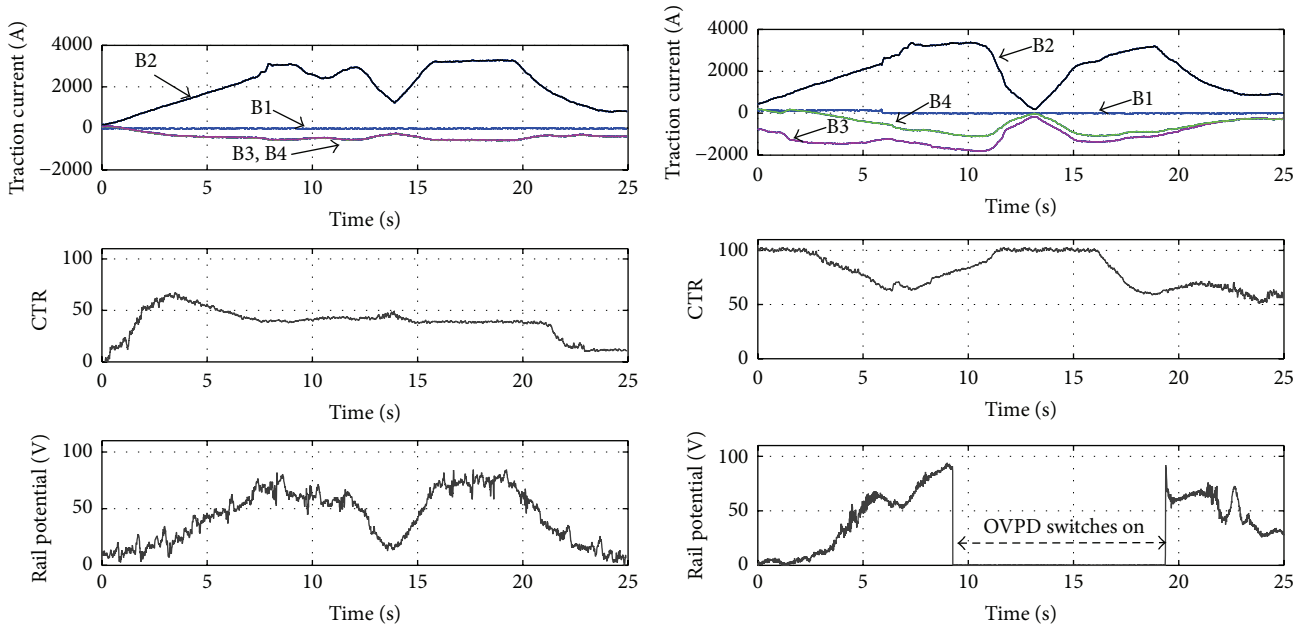
(a) Traction current and rail potential when Tr4 accelerates

(b) Traction current and rail potential when Tr5 accelerates
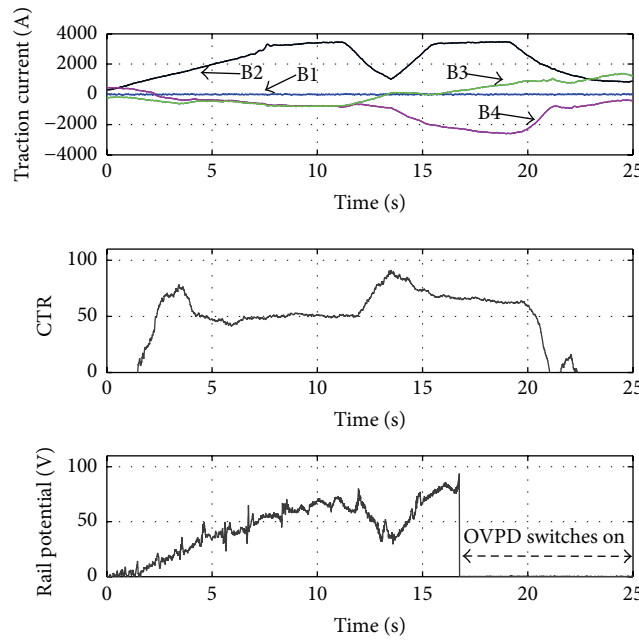
(c) Traction current and rail potential when Tr6 accelerates

FIGURE 7: Test results of traction current and rail potential.

time $i_r(x, t)$, and the stray current in buried conductor at each position changing with time $i_s(x, t)$ need to be calculated.

The distribution of $u_r(x)$, $u_s(x)$, $i_r(x)$, $i_s(x)$ at a certain movement can be calculated as follows.

4.1. Modification of Equivalent Reflux Parameters. The distributed parameters of reflux system must be converted to lumped parameters for the calculation of power flow, and

then, rail potential and stray current can be assessed in the distributed parameter model on basis of boundary conditions calculated by power flow. The distributed parameter model and the equivalent lumped parameter model are shown in Figure 8.

For the realization of fast and accurate calculation, modification of reflux system parameters is proposed based on lumped parameter model and distributed parameter model of the reflux system.
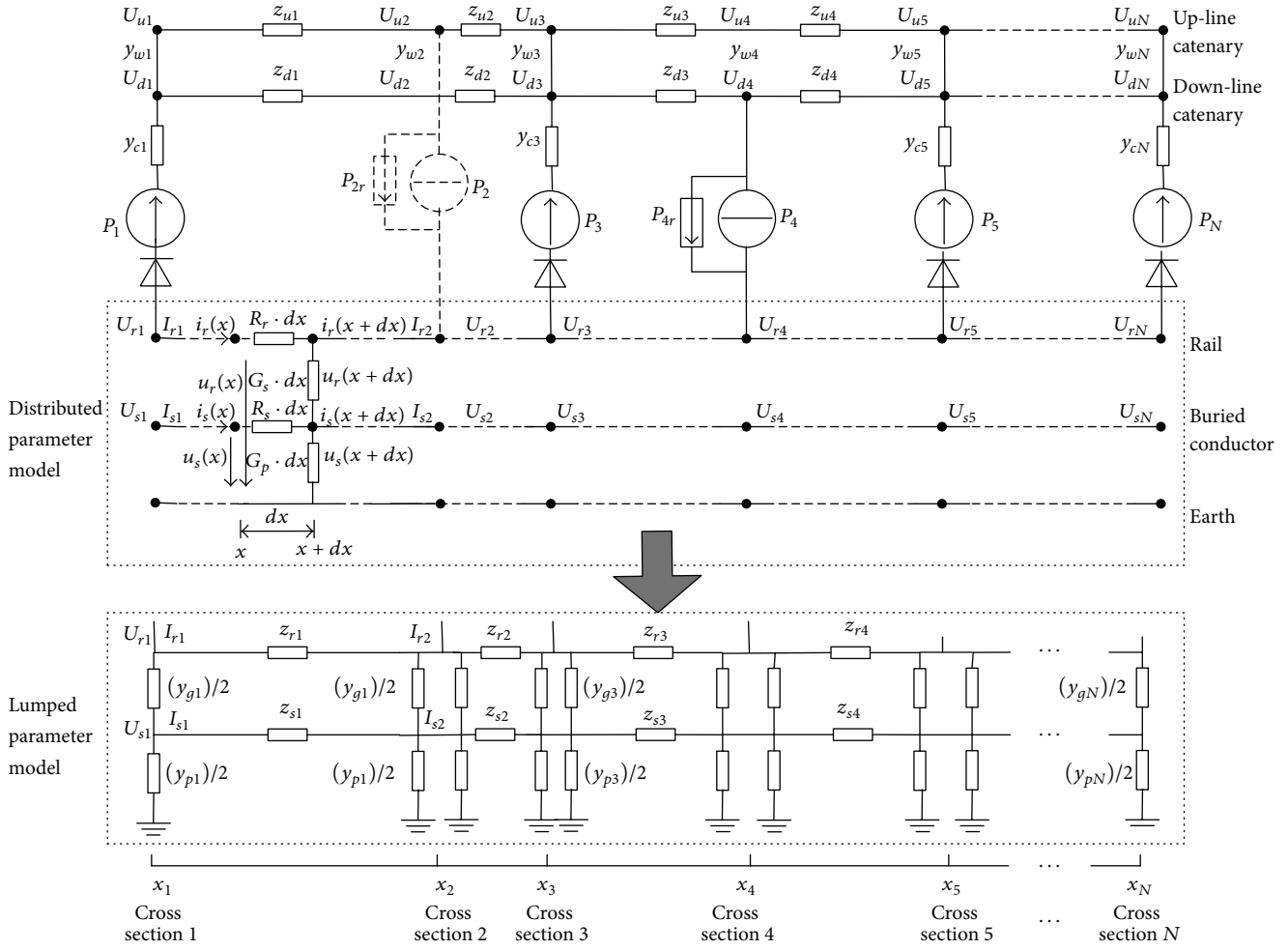
FIGURE 8: Model of DC traction power system.

Distributed parameter model of reflux system is shown in Figure 8 and $u_r(x)$, $u_s(x)$, $i_r(x)$, and $i_s(x)$ at x in the distributed parameter model are derived from Kirchhoff's law [2, 9, 12] as follows:

$$\frac{du_r(x)}{dx} = -R_r \cdot i_r(x),$$

$$\frac{du_s(x)}{dx} = -R_s \cdot i_s(x),$$

$$\frac{di_r(x)}{dx} = -G_s \cdot u_r(x) + G_s \cdot u_s(x),$$

$$\frac{di_s(x)}{dx} = G_s \cdot u_r(x) - (G_p + G_s) \cdot u_s(x),$$

(2)

where R_r is longitudinal resistance of the rail, R_s is longitudinal resistance of the buried conductor, G_s is longitudinal insulation conductance of rail to buried conductor, and G_p is longitudinal insulation conductance of buried conductor to earth.

Solutions of differential equations are shown in the following:

$$\begin{bmatrix} u_r(x) \\ u_s(x) \\ i_r(x) \\ i_s(x) \end{bmatrix} = \mathbf{H} \begin{bmatrix} C_1 e^{-\alpha x} \\ C_2 e^{\alpha x} \\ C_3 e^{-\beta x} \\ C_4 e^{\beta x} \end{bmatrix},$$

(3)

where

$$\mathbf{H} = \begin{bmatrix} 1 & 1 & 1 & 1 \\ \dfrac{\alpha}{R_r} & -\dfrac{\alpha}{R_r} & \dfrac{\beta}{R_r} & -\dfrac{\beta}{R_r} \\ 1 - \dfrac{\alpha^2}{G_s R_r} & 1 - \dfrac{\alpha^2}{G_s R_r} & 1 - \dfrac{\beta^2}{G_s R_r} & 1 - \dfrac{\beta^2}{G_s R_r} \\ r_\alpha & -r_\alpha & r_\beta & -r_\beta \end{bmatrix},$$

$$r_\alpha = \frac{G_p}{\alpha} - \frac{\alpha}{R_r} - \frac{G_p \alpha}{G_s R_r},$$

$$r_\beta = \frac{G_p}{\beta} - \frac{\beta}{R_r} - \frac{G_p \beta}{G_s R_r},$$

$$\alpha = \sqrt{\frac{m+n}{2} + \sqrt{\frac{(m-n)^2}{4} + mk}},$$

$$\beta = \sqrt{\frac{m+n}{2} - \sqrt{\frac{(m-n)^2}{4} + mk}},$$

$$m = G_s R_r,$$

$$n = R_s (G_s + G_p),$$

$$k = R_s G_s,$$

$$(4)$$

and $C_1 \sim C_4$ can be obtained from the boundary conditions at $x = x_1$ and $x = x_2$. In the distributed parameter model, at the position $x = x_1$, the boundary conditions are $u_r(x_1) = U_{r1}$, $u_s(x_1) = U_{s1}$, $i_r(x_1) = I_{r1}$, and $i_s(x_1) = I_{s1}$.

So, at position $x = x_1$,

$$\mathbf{H} \begin{bmatrix} C_1 e^{-\alpha x_1} \\ C_2 e^{\alpha x_1} \\ C_3 e^{-\beta x_1} \\ C_4 e^{\beta x_1} \end{bmatrix} = \begin{bmatrix} U_{r1} \\ U_{s1} \\ I_{r1} \\ I_{s1} \end{bmatrix}. \tag{5}$$

Then,

$$\begin{bmatrix} C_1 \\ C_2 \\ C_3 \\ C_4 \end{bmatrix} = \mathbf{H}^{-1} \begin{bmatrix} U_{r1} \\ U_{s1} \\ I_{r1} \\ I_{s1} \end{bmatrix} \begin{bmatrix} e^{\alpha x_1} & e^{-\alpha x_1} & e^{\beta x_1} & e^{-\beta x_1} \end{bmatrix}$$

$$= \begin{bmatrix} e^{\alpha x_1} (h_{11} U_{r1} + h_{12} U_{s1} + h_{13} I_{r1} + h_{14} I_{s1}) \\ e^{-\alpha x_1} (h_{21} U_{r1} + h_{22} U_{s1} + h_{23} I_{r1} + h_{24} I_{s1}) \\ e^{\beta x_1} (h_{31} U_{r1} + h_{32} U_{s1} + h_{33} I_{r1} + h_{34} I_{s1}) \\ e^{-\beta x_1} (h_{41} U_{r1} + h_{42} U_{s1} + h_{43} I_{r1} + h_{44} I_{s1}) \end{bmatrix},$$

$$(6)$$

where $h_{11} \sim h_{44}$ are elements of $\mathbf{H}^{-1}$.

At the position $x = x_2$, I_{r2} can be expressed as follows:

$$I_{r2} = \left(1 - \frac{\alpha^2}{G_s R_r}\right) C_1 e^{-\alpha x_2} + \left(1 - \frac{\alpha^2}{G_s R_r}\right) C_2 e^{\alpha x_2}$$

$$+ \left(1 - \frac{\beta^2}{G_s R_r}\right) C_3 e^{-\beta x_2} + \left(1 - \frac{\beta^2}{G_s R_r}\right) C_4 e^{\beta x_2} \tag{7}$$

$$= k_1 U_{r1} + k_2 U_{s1} + k_3 I_{r1} + k_4 I_{s1}.$$

Based on the system parameters, k_1, k_2, k_3, and k_4 are the function of segment length $(x_2 - x_1)$.

In the lumped parameter model shown in Figure 8, I_{r2} can be expressed as follows:

$$I_{r2} = U_{r1} \left[\frac{y_{g1}}{2} + \frac{y_{g1}}{2} + \frac{y_{g1}^2 z_{r1}}{4} + \frac{y_{g1}^2 z_{s1}}{4} \right] - U_{s1} \left[\frac{y_{g1}}{2} \right.$$

$$+ \frac{y_{g1}}{2} + \frac{y_{g1}^2 z_{r1}}{4} + \frac{y_{g1}^2 z_{s1}}{4} + \frac{y_{g1} y_{p1} z_{s1}}{4} \right] + I_{r1} \left[1 \right. \tag{8}$$

$$\left. + \frac{y_{g1} z_{r1}}{2} \right] - I_{s1} \left[\frac{y_{g1} z_{s1}}{2} \right].$$

The equivalent lumped parameters of the reflux system can be expressed as follows according to (8) and (7):

$$\frac{y_{g1}}{2} = \frac{k_1}{1 + k_3 + k_4},$$

$$z_{r1} = \frac{(k_3 - 1)(k_4 + k_3 + 1)}{k_1},$$

$$\frac{y_{p1}}{2} = \frac{k_2 - k_1}{k_4}, \tag{9}$$

$$z_{s1} = \frac{k_4 (1 + k_3 + k_4)}{k_1}.$$

The lumped parameters in each section of Figure 8 can be updated by the length L of the section based on (9).

With this modification method, the distributed parameter model of reflux system between two cross sections can be equivalent to lumped parameter model. In this process, voltage and current at the ports keep constant to ensure the accuracy of the equivalent parameters.

4.2. Flow Calculation Based on Unified Chain Model

4.2.1. Model Description. A huge number of nodes exist in the model shown in Figure 8. The admittance matrix of the model will be changed in flow calculation with different operation modes of the traction substation and train. On basis of chain model in AC traction power system [20, 21], equivalent chain model of DC traction power system divided by cross section is shown in Figure 9.

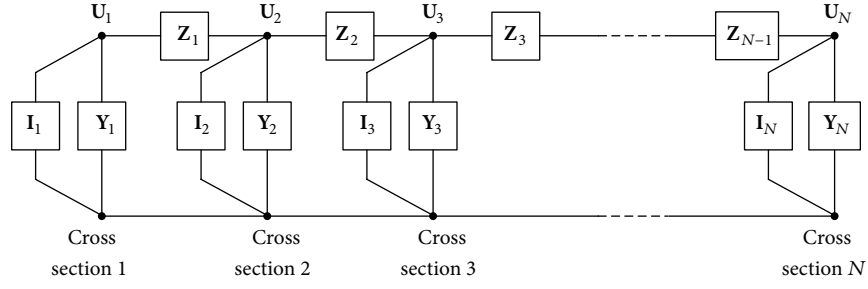Nodal voltage equation of the chain model is shown as follows:

FIGURE 9: Chain model of DC traction power system.

$$
\begin{bmatrix}
\mathbf{Y}_1 + \mathbf{Z}_1^{-1} & -\mathbf{Z}_1^{-1} \\
-\mathbf{Z}_1^{-1} & \mathbf{Z}_1^{-1} + \mathbf{Y}_2 + \mathbf{Z}_2^{-1} & -\mathbf{Z}_2^{-1} \\
 & -\mathbf{Z}_2^{-1} & \mathbf{Z}_2^{-1} + \mathbf{Y}_3 + \mathbf{Z}_3^{-1} & -\mathbf{Z}_3^{-1} \\
 & & \ddots & \ddots & \ddots \\
 & & & -\mathbf{Z}_{N-1}^{-1} & \mathbf{Z}_{N-1}^{-1} + \mathbf{Y}_N
\end{bmatrix}
\begin{bmatrix}
\mathbf{U}_1 \\ \mathbf{U}_2 \\ \mathbf{U}_3 \\ \vdots \\ \mathbf{U}_N
\end{bmatrix}
=
\begin{bmatrix}
\mathbf{I}_1 \\ \mathbf{I}_2 \\ \mathbf{I}_3 \\ \vdots \\ \mathbf{I}_N
\end{bmatrix}.
\tag{10}
$$

The submatrixes in (10) can be defined as follows:

$$
\mathbf{Y}_n =
\begin{bmatrix}
y_{wn} + y_{cn} & -y_{wn} & -y_{cn} & 0 & U_{bn} \\
-y_{wn} & y_{wn} & 0 & 0 & 0 \\
-y_{cn} & 0 & y_{cn} + \dfrac{y_{g(n-1)} + y_{gn}}{2} & \dfrac{-y_{g(n-1)} - y_{gn}}{2} & -U_{bn} \\
0 & 0 & \dfrac{-y_{g(n-1)} - y_{gn}}{2} & \dfrac{y_{g(n-1)} + y_{gn} + y_{p(n-1)} + y_{pn}}{2} & 0 \\
b_{rn} & 0 & -b_{rn} & 0 & 0
\end{bmatrix},
\tag{11}
$$

$$
\mathbf{Z}_n^{-1} = \mathrm{diag}\left(\frac{1}{z_{dn}}, \frac{1}{z_{un}}, \frac{1}{z_{rn}}, \frac{1}{z_{sn}}, 0 \right),
\tag{12}
$$

$$
\mathbf{U}_n = [U_{dn}; U_{un}; U_{rn}; U_{sn}; y_{zn}],
\tag{13}
$$

$$
\mathbf{I}_n = [I_{dn}; I_{un}; I_{rn}; I_{sn}; U_{bn}].
\tag{14}
$$

At the cross section n ($1 < n < N$), the unified admittance submatrix $\mathbf{Y}_n$ can be defined as (11). y_{wn} is a state variable of the node type, $y_{wn} = 0$ indicates that this is a cross section of train, and the catenaries of up-line and down-line are independent. $y_{wn} = 1e5$ indicates that this is a cross section of traction substation, and the catenaries of up-line and down-line are connected with each other. y_{cn} is self-admittance of the power source at cross section n. At the cross section of train, $y_{cn} = 0$, and at the cross section of traction substation, $y_{cn} = 1/R_{eq}$. y_{gn} and y_{pn} can be obtained by (9) with the length of segment from cross section n to cross section $(n + 1)$. b_{rn} is a state variable of train's running mode, $b_{rn} = 1$ indicates that the train is in regenerative braking, and the energy absorbing device is in operation; otherwise, $b_{rn} = 0$. U_{bn} is the limited voltage $U_{\lim}$. $y_{g(n-1)} =$

$y_{p(n-1)} = 0$ at cross section $n = 1$, and $y_{gn} = y_{pn} = 0$ at cross section $n = N$.

The submatrix of multiconductor impedance between cross section n and cross section $(n + 1)$ ($1 \leq n < N$) $\mathbf{Z}_n$ can be defined as (12), where $z_{dn} = z_{un} = (x_{(n+1)} - x_n)R_w$, R_w is the longitudinal resistance of the catenary. z_{rn} and z_{sn} can be modified by (9) with $(x_{(n+1)} - x_n)$.

At the cross section n ($1 \leq n \leq N$), the unified submatrix of node voltage $\mathbf{U}_n$ can be defined as (13). y_{zn} is the admittance of the energy absorbing device which can keep the voltage of the catenary in $U_{\lim}$ at the cross section of train. U_{dn}, U_{un}, U_{sn}, and U_{rn}, respectively, represent the voltage of down-line catenary to earth, voltage of up-line catenary to earth, voltage of rail to earth, and voltage of buried conductor to earth at cross section n.

At the cross section n ($1 \leq n \leq N$), the unified submatrix of node current-injection $\mathbf{I}_n$ can be defined as (14). I_{dn}, I_{un}, I_{rn}, and I_{sn}, respectively, represent the current-injection of down-line catenary node, current-injection of up-line catenary node, current-injection of rail node, and current-injection of the buried conductor node. U_{bn} is consistent with that in (11).

The complicated operation modes of train and traction substation can be unified by the submatrix (11)~(14), and the flow calculation can be efficient.

4.2.2. Flow Calculation by Unified Chain Model. At a certain movement, the flow calculation of DC traction power system can be carried out using iterative methods based on (10). At the step $i = 1$, the traction substations are out of operation and $\mathbf{U}_n^{(1)} = [U_0; U_0; 0; 0; 0]$. At cross section of traction substation, $\mathbf{I}_n^{(1)} = [U_0/R_{eq}; 0; -U_0/R_{eq}; 0; 0]$. At cross section of up-line train, $\mathbf{I}_n^{(1)} = [0; P_n/(U_{un}^{(1)} - U_{rn}^{(1)}); -P_n/(U_{un}^{(1)} - U_{rn}^{(1)}); 0; 0]$, while at cross section of down-line train, $\mathbf{I}_n^{(1)} = [P_n/(U_{un}^{(1)} - U_{rn}^{(1)}); 0; -P_n/(U_{un}^{(1)} - U_{rn}^{(1)}); 0; 0]$. P_n is the power of the train at cross section n in this movement. $\mathbf{U}_n^{(2)}$ can be obtained by (10) from $\mathbf{G}_n^{(1)} \mathbf{U}_n^{(2)} = \mathbf{I}_n^{(1)}$ and then the coefficient matrix $\mathbf{G}^{(2)}$ and current-injection submatrix $\mathbf{I}_n^{(2)}$ can be updated based on $\mathbf{U}_n^{(2)}$. The iteration will continue until the step i when $\mathbf{U}_n^{(i)} - \mathbf{U}_n^{(i-1)}$ at each cross section is lower than the voltage convergence precision ξ.

The changes of the submatrixes in the iteration are shown as follows.

In the i step at cross section n of traction substation, when $U_{dn}^{(i)} - U_{rn}^{(i)} < U_0$, $y_{wn} = 1e5$, $y_{cn} = 1/R_{eq}$, $U_{bn} = 0$, and $\mathbf{I}_n = [U_0/R_{eq}; 0; -U_0/R_{eq}; 0; 0]$, and when $U_{dn}^{(i)} - U_{rn}^{(i)} \geq U_0$, $y_{wn} = 1e5$, $y_{cn} = 0$, $\mathbf{I}_n = [0; 0; 0; 0; 0]$, $U_{bn} = 0$, and $b_n = 0$.

In the i step at cross section m of train, when $U_{dm}^{(i)} - U_{rm}^{(i)} < U_{\lim}$, then $y_{wm} = 0$, $y_{cm} = 0$, $b_n = 0$, and $U_{bn} = 0$; when $U_{dm}^{(i)} - U_{rm}^{(i)} \geq U_{\lim}$, then $y_{wm} = 0$, $y_{cm} = 0$, $b_n = 1$, and $U_{bn} = U_{\lim}$. When the train is in up-line, $\mathbf{I}_m = [0; P_m/(U_{um}^{(i)} - U_{rm}^{(i)}); -P_m/(U_{um}^{(i)} - U_{rm}^{(i)}); 0; 0]$, and when the train is in down-line, $\mathbf{I}_m = [P_m/(U_{dm}^{(i)} - U_{rm}^{(i)}); 0; -P_m/(U_{dm}^{(i)} - U_{rm}^{(i)}); 00]$. P_m is train's power in this moment.

After the flow calculation, $\mathbf{U}_n$ and $\mathbf{I}_n$ at each cross section can be obtained and be used as boundary conditions for the calculation of rail potential and stray current.

4.3. Distribution of Rail Potential and Stray Current. The rail potential, potential of buried conductor, current in rail, and stray current in cross section n to cross section $(n + 1)$ ($1 \leq n < N$) are, respectively, defined as $u_{rn}(x)$, $u_{sn}(x)$, $i_{rn}(x)$, and $i_{sn}(x)$. They can be expressed as follows:

$$
\begin{bmatrix} u_{rn}(x) \\ u_{sn}(x) \\ i_{rn}(x) \\ i_{sn}(x) \end{bmatrix} = \mathbf{H} \begin{bmatrix} C_{n1}e^{-\alpha x} \\ C_{n2}e^{\alpha x} \\ C_{n3}e^{-\beta x} \\ C_{n4}e^{\beta x} \end{bmatrix},
\tag{15}
$$

where $x_n \leq x \leq x_{(n+1)}$ and $\mathbf{H}$ is shown in (3).

The boundary conditions of the model can be obtained at $x = x_n$, and $x = x_{(n+1)}$. At $x = x_n$, $u_{rn}(x_n) = U_{rn}$, $u_{sn}(x_n) = U_{sn}$. At $u_{rn}(x_{(n+1)}) = U_{r(n+1)}$, and $u_s(x_{(n+1)}) = U_{s(n+1)}$.

Then $C_{n1} \sim C_{n4}$ can be obtained as follows:

$$
\begin{bmatrix} C_{n1} \\ C_{n2} \\ C_{n3} \\ C_{n4} \end{bmatrix} = \mathbf{M}^{-1} \begin{bmatrix} U_{rn} \\ U_{sn} \\ U_{r(n+1)} \\ U_{s(n+1)} \end{bmatrix},
\tag{16}
$$

where

$$
\mathbf{M} = \begin{bmatrix}
e^{\alpha x_n} & e^{-\alpha x_n} & e^{\beta x_n} & e^{-\beta x_n} \\
\dfrac{\alpha}{R_r}e^{\alpha x_n} & -\dfrac{\alpha}{R_r}e^{-\alpha x_n} & \dfrac{\beta}{R_r}e^{\beta x_n} & -\dfrac{\beta}{R_r}e^{-\beta x_n} \\
e^{\alpha x_{(n+1)}} & e^{-\alpha x_{(n+1)}} & e^{\beta x_{(n+1)}} & e^{-\beta x_{(n+1)}} \\
\dfrac{\alpha}{R_r}e^{\alpha x_{(n+1)}} & -\dfrac{\alpha}{R_r}e^{-\alpha x_{(n+1)}} & \dfrac{\beta}{R_r}e^{\beta x_{(n+1)}} & -\dfrac{\beta}{R_r}e^{-\beta x_{(n+1)}}
\end{bmatrix}.
\tag{17}
$$

The distribution of rail potential and stray current in multitrains and multisubstations at a certain movement can be simulated. Based on $p(t)$ and $x(t)$ of the trains in line at each movement, $u_r(x,t)$, $u_s(x,t)$, $i_r(x,t)$, and $i_s(x,t)$ can be simulated.

5. Simulation Results

Simulations of rail potential and stray current affected by over zone feeding are presented in this paper. Parameters of the equivalent model in the simulations are as follows: no-load voltage of the traction substation $U_0 = 1593\,\text{V}$, equivalent resistance of the traction substation $R_{eq} = 0.054\,\Omega$, trigger voltage of the regenerative energy absorbing device $U_{\lim} = 1800\,\text{V}$, $R_w = 0.01\,\Omega/\text{km}$, $R_r = 0.03\,\Omega/\text{km}$, $R_s = 0.02\,\Omega/\text{km}$, $G_s = 0.2\,\text{S/km}$, and $G_p = 0.2\,\text{S/km}$, and the voltage convergence precision in the iteration $\xi = 0.01\,\text{V}$. Configuration and technical parameters used for train movement calculation are provided by Guangzhou Metro Line 8 and the time step in train movement calculation is 0.2 s. There are two trains (Tr1, Tr2) running in line powered by three traction substations (Station A, Station B, and Station C) with the positions $S_A = 0\,\text{m}$, $S_B = 2000\,\text{m}$, and $S_C = 4000\,\text{m}$ in the simulation model. OVPD is not set in the model.

5.1. Analysis of Over Zone Feeding. Multitrains and multisubstations are in parallel operation in DC traction power system. Simulations and analysis of over zone feeding have been carried out in this paper.

In the simulation, two trains run in the line from Station A to Station C, and the dwell time at Station B is 30.0 s. The starting times of Tr1 and Tr2 from Station A to Station C are, respectively, 0.0 s and 220.0 s. The powers and positions of Tr1 and Tr2 obtained from the train movement calculation, $P_1(t)$, $P_2(t)$, $S_1(t)$, and $S_2(t)$, are shown in Figure 10(a). Tr1
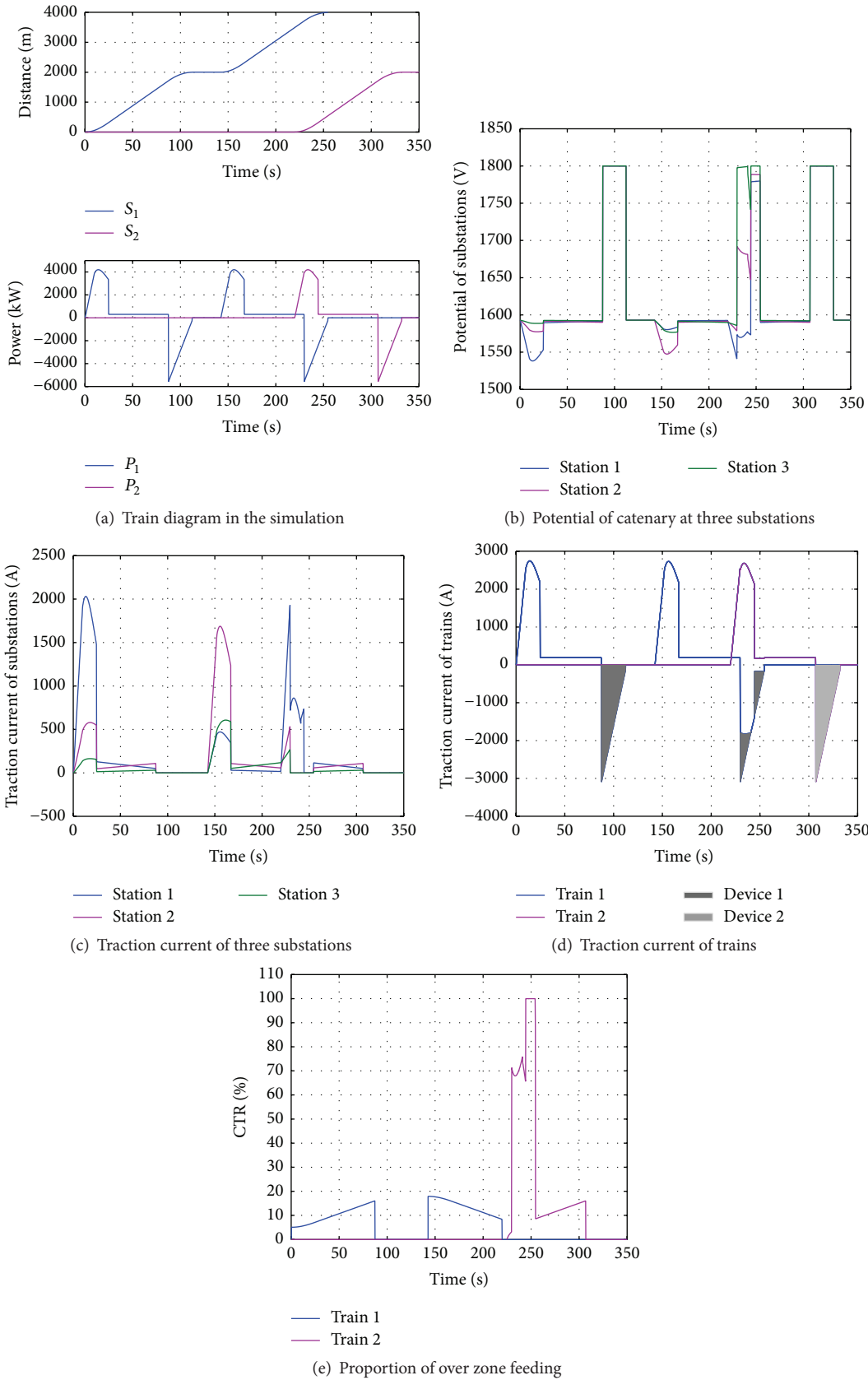
(a) Train diagram in the simulation

(b) Potential of catenary at three substations

(c) Traction current of three substations

(d) Traction current of trains

(e) Proportion of over zone feeding

FIGURE 10: Simulation results of over zone feeding.

(a) Variation of rail potential

(b) Potential of buried conductor

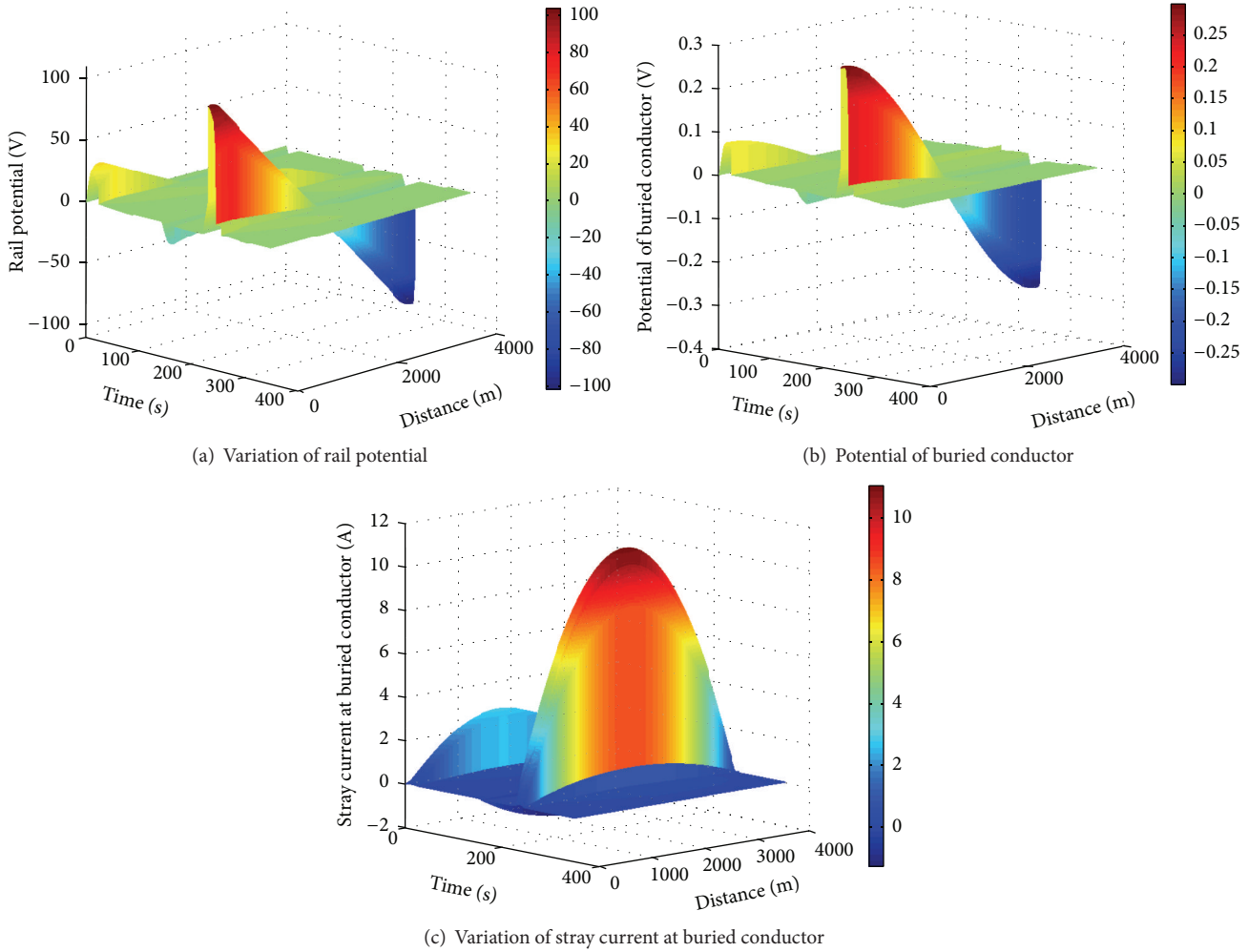(c) Variation of stray current at buried conductor

FIGURE 11: Simulation results of rail potential and stray current.

arrives at Station B at the time 112.2 s and runs from Station B to Station C after 30.0 s dwell. Tr2 runs from Station A to Station B during the time of 220.0 s~332.2 s. The variation of potential and current at the traction substations and trains are shown in Figures 10(b)~10(e).

As shown in Figure 10, when Tr1 accelerates from Station A during 0.0 s~87.4 s, train current of Tr1 comes from three traction substations with different proportions. The proportion of traction current coming from over zone feeding changes with the position of Tr1, but in a low amplitude from 5.07% to 16.03%. When Tr1 begins regenerative braking at 87.4 s, the potential of catenary rises rapidly to 1800 V and the regenerative energy absorbing device on Tr1 is activated to absorb the energy. When Tr2 accelerates from Station A to Station B from 220.0 s to 229.6 s, potentials and currents of three substations are consistent with the process of Tr1. From the time 229.6 s to 254.6 s, regenerative braking of Tr1 has a significant impact on simulation results. Most of the regenerative current of Tr1 is fed back to the catenary and supplied to Tr2; meanwhile, the current coming from traction substations decreases greatly. At 229.8 s, the distance between Tr1 and Tr2 is 3656.6 m and traction current of

Tr2 is 2506.0 A. Regenerative current of Tr1 is 3094.0 A, and 1788.0 A of which is supplied for Tr2. The proportion of traction current coming from over zone feeding in Tr2 is 71.3%. In this case, the length of current transmission for Tr2 is much longer than that when Tr1 accelerates from Station A to Station B. The maximum current of over zone feeding is 1824.4 A at 234.4 s, in which time the distance between Tr1 and Tr2 is 3686.4 m. When the potential of catenary reaches the $U_{\lim}$ at the position of Tr2, the rest of regenerative current will be absorbed by the energy absorbing device on the train. Simulation results show that traction current coming from over zone feeding is greatly affected by the running modes of multitrains and the regenerative energy saving devices.

5.2. Effects of Over Zone Feeding on Rail Potential and Stray Current.
Field tests and simulation results show that over zone feeding will increase the length of traction current transmission. Simulations of rail potential and stray current affected by over zone feeding have been carried out with the train diagram shown in Figure 10(a). The variation of rail potential, potential of buried conductor, and stray current are shown in Figure 11.
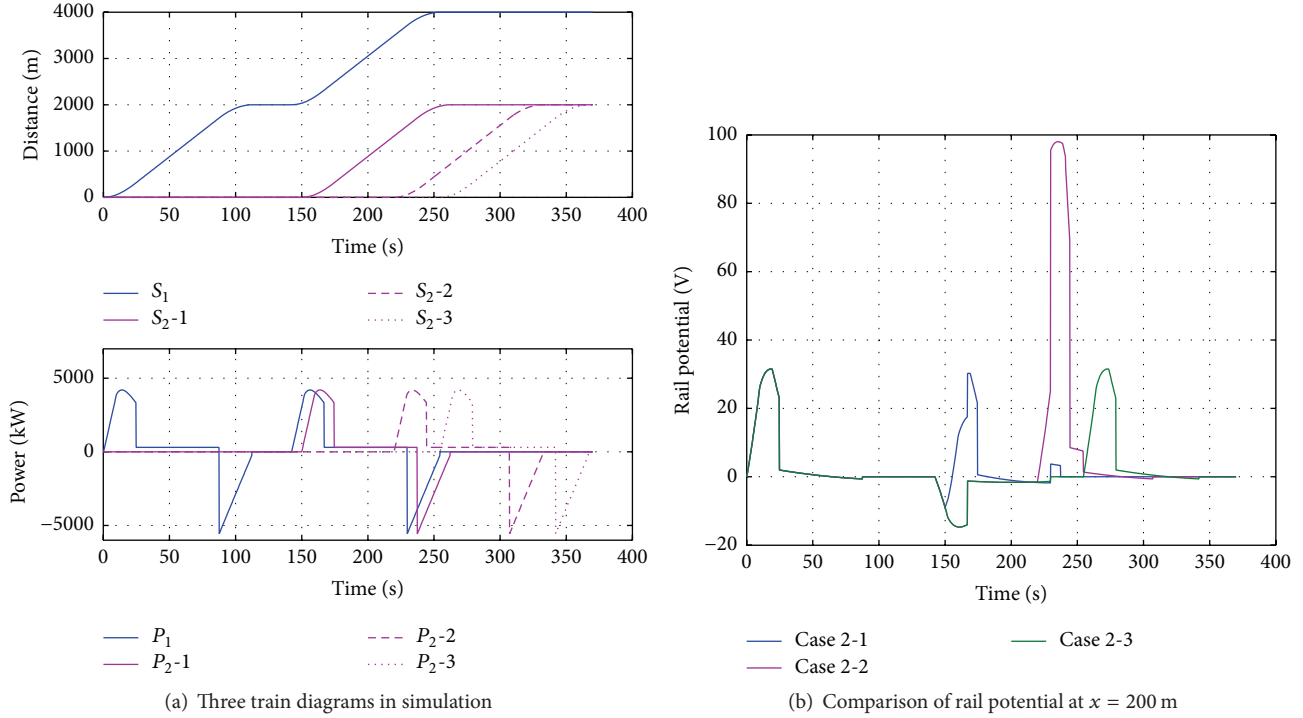
(a) Three train diagrams in simulation

(b) Comparison of rail potential at $x = 200$ m

FIGURE 12: Comparison of rail potential in different train diagrams.

TABLE 4: Summary of simulation results for different diagrams ($x = 200$ m).

Items	Cases		
	S_2-1	S_2-2	S_2-3
Max. rail potential (V)	30.26	98.00	31.53
Max. stray current (A)	0.64	2.37	0.71
Max. buried conductor potential (V)	0.08	0.29	0.08
Traction current of train (A)	2624.0	2659.0	2600.1
CTR of train current (%)	5.6	68.58	6.3

Figure 11(a) shows the rail potential at each position changing with time. At the same position, such as $x = 0$ m, the rail potential when Tr2 accelerates from 220.0 s to 244.6 s is much higher than that when Tr1 accelerates from 0.0 s to 24.6 s. The highest rail potential occurs at the position of the train. The potential of buried conductor illustrated in Figure 11(b) shows the same trend as Figure 11(a). In Figure 11(c), stray current with larger proportion of current coming from over zone feeding is much higher than that with a lower proportion, and the highest stray current occurs at the middle of Tr1 and Tr2. Figures 11(a)~11(c) show that over zone feeding has a great impact on rail potential and stray current.

The extent of over zone feeding will be changed in different train diagrams. As shown in Figure 12(a), three diagrams are set in the simulation. In the diagrams Tr2 starts at 150.0 s, 220.0 s, and 254.6 s, respectively. Figure 12(b) shows the simulation results of rail potential at $x = 200$ m in different diagrams.

Summary of simulation results on rail potential is shown in Table 4. Comparing the simulation results at $x = 200$ m in three diagrams, significant differences of maximum rail potential and stray current exist with different extent of over zone feeding. Maximum rail potential is 98.00 V when Tr2 runs with the diagram S_2-2. At this point of time, the traction current of Tr2 is 2659.0 A, 68.58% of which comes from over zone feeding. As a comparison, maximum rail potentials are 30.26 V and 31.53 V, respectively, when Tr2 runs with diagrams S_2-1 and S_2-3.

Extent of over zone feeding also can be changed by different starting voltage of the regenerative energy absorbing device. Three cases are set in the simulation with different U_{lim} in the same train diagram shown in Figure 10(a). In Case 1 and Case 2, U_{lim} are 1800 V and 1700 V, respectively, and in Case 3, the regenerative energy is all absorbed by energy saving device on the train instead of being fed back to the catenary. Figure 13 shows the simulation results in three cases.

Figure 13(a) shows the proportions of traction current coming from over zone feeding in three cases when Tr2 runs from Station A to Station B. From 244.4 s to 254.4 s, CTR of Case 1 and Case 2 are in the same value. CTR of Case 1, Case 2, and Case 3 is the same from 254.4 s to 350 s. In acceleration process of Tr2 from 229.8 s to 244.4 s, CTR of Case 1 is the highest of the three cases; therefore, the traction current comes from over zone feeding for Tr1 is the highest. Figure 13(b) shows that the maximum amplitude of traction current coming from over zone feeding in three cases is 1903.1 A, 1240.4 A, and 167.6 A, respectively, with the same distance of transmission. Figure 13(c) shows the simulation results of rail potential at $x = 200$ m in three cases. Maximum

(a) CTR in different cases

(b) Current from over zone feeding in different cases

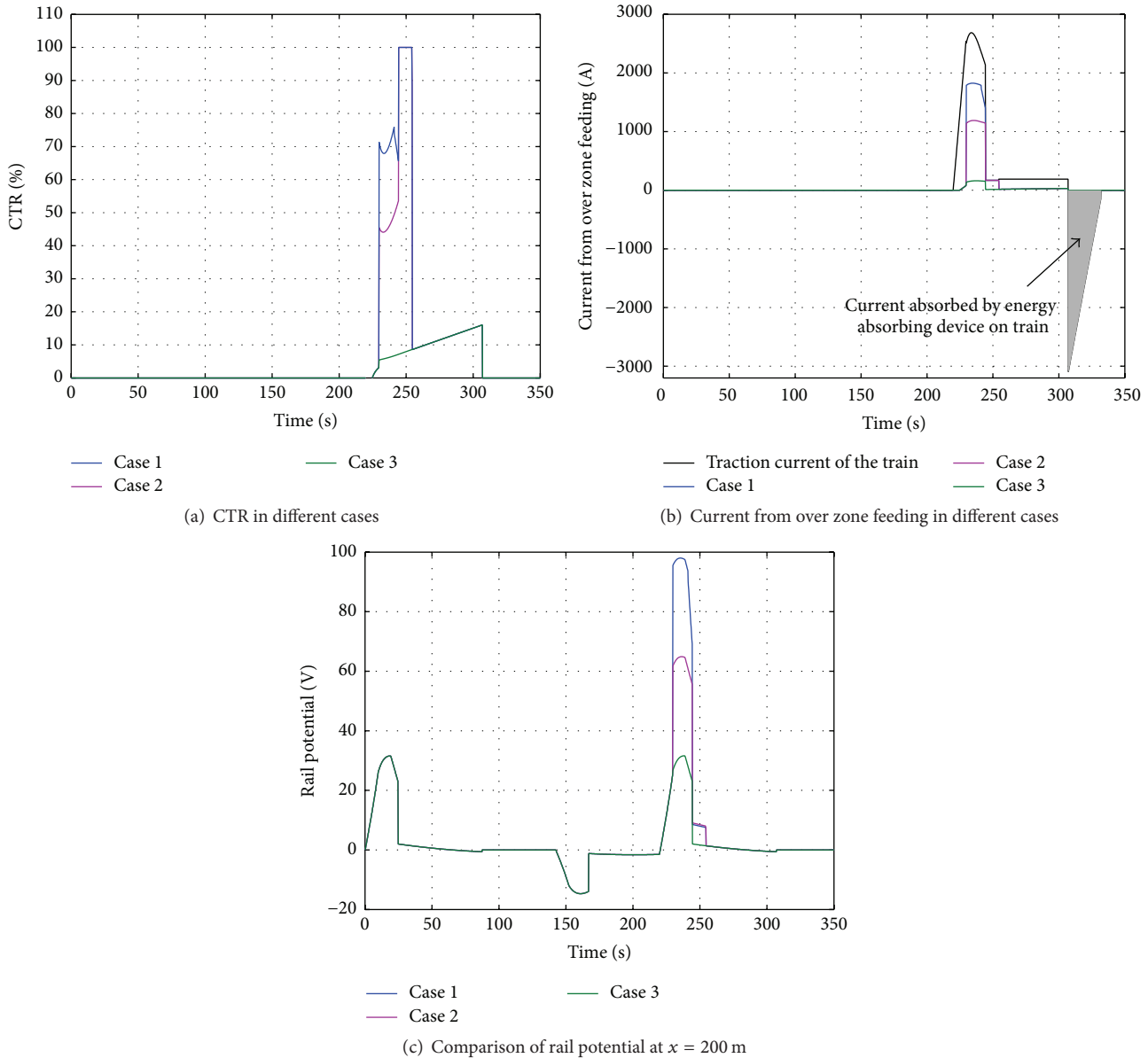(c) Comparison of rail potential at $x = 200$ m

FIGURE 13: Comparison of rail potential in different cases.

rail potentials in Case 1, Case 2, and Case 3 are 98.00 V, 64.89 V, and 31.59 V, respectively, and maximum stray current at $x = 200$ m in three cases is 2.37 A, 1.54 A, and 0.71 A, respectively.

On basis of the simulation results, rail potential and stray current are highly influenced by the extent of over zone feeding which can be changed by train diagrams or different starting voltage of the regenerative energy absorbing device.

6. Summary and Conclusion

In this paper, influence of over zone feeding on rail potential and stray current has been proposed in DC mass transit system and results of field tests and simulations have been presents. Conclusions can be drawn as follows:

(1) The phenomenon of over zone feeding exists widely in DC mass transit system for electrical connectivity of the catenary. Extent of over zone feeding is related to the running mode of the trains in line, and it will be exacerbated when the braking energy fed back to the catenary is absorbed by other running trains. In extreme cases, all traction current of the accelerating train comes from the energy fed back by the braking train. When the braking energy fed back to the catenary surpasses the absorption capability of other running trains, voltage of the catenary will increase rapidly, therefore, triggering the energy saving device.

(2) Rail potential and stray current are highly related to over zone feeding, which will be higher when the extent of over zone feeding is exacerbated in the same

traction current of the train. According to the simulating results, the maximum rail potential is 31.53 V when the proportion of traction current coming from over zone feeding is 6.3%, while the maximum rail potential is 98.00 V when the proportion is 68.58%.

(3) The extent of over zone feeding will be changed by different train diagrams or different starting voltage of the energy absorbing device and these methods can be applied to the control of rail potential and stray current.

(4) The dynamic analysis model proposed in this paper can be effectively used in analyzing the effect of over zone feeding on rail potential and stray current with multiple trains running in multiple zones.

Conflict of Interests

The authors declare that there is no conflict of interests regarding the publication of this paper.

Acknowledgments

References

[1] J. G. Yu and C. J. Goodman, "Modelling of rail potential rise and leakage current in DC rail transit systems," in *Proceedings of the IEE Colloquium on Stray Current Effects of DC Railways and Tramways*, London, UK, October 1990.

[2] J. G. Yu, "The effects of earthing strategies on rail potential and stray currents in DC transit railways," in *Proceedings of the International Conference on Developments in Mass Transit Systems*, Conference Publication no. 453, pp. 303–309, London, UK, April 1998.

[3] C.-H. Lee and H.-M. Wang, "Effects of grounding schemes on rail potential and stray currents in Taipei Rail Transit Systems," *IEE Proceedings: Electric Power Applications*, vol. 148, no. 2, pp. 148–154, 2001.

[4] I. Cotton, C. Charalambous, P. Aylott, and P. Ernst, "Stray current control in DC mass transit systems," *IEEE Transactions on Vehicular Technology*, vol. 54, no. 2, pp. 722–730, 2005.

[5] W. Ping, "Analysis on rail potential in transit," *Modern Urban Transit*, no. 2, pp. 67–73, 2014.

[6] M. Yinshan, "Frame protection breakdown caused by refusing action of rail potential limit equipment," *Urban Rapid Rail Transit*, no. 3, pp. 92–94, 2008.

[7] Y. C. Liu and J. F. Chen, "Control scheme for reducing rail potential and stray current in MRT systems," *IEE Proceedings-Electric Power Applications*, vol. 152, no. 3, pp. 612–618, 2005.

[8] C.-H. Lee, "Evaluation of the maximum potential rise in Taipei rail transit systems," *IEEE Transactions on Power Delivery*, vol. 20, no. 2, pp. 1379–1384, 2005.

[9] C.-H. Lee and C.-J. Lu, "Assessment of grounding schemes on rail potential and stray currents in a DC transit system," *IEEE Transactions on Power Delivery*, vol. 21, no. 4, pp. 1941–1947, 2006.

[10] Y.-S. Tzeng and C.-H. Lee, "Analysis of rail potential and stray currents in a direct-current transit system," *IEEE Transactions on Power Delivery*, vol. 25, no. 3, pp. 1516–1525, 2010.

[11] S.-L. Chen, S.-C. Hsu, C.-T. Tseng, K.-H. Yan, H.-Y. Chou, and T.-M. Too, "Analysis of rail potential and stray current for Taipei Metro," *IEEE Transactions on Vehicular Technology*, vol. 55, no. 1, pp. 67–75, 2006.

[12] S.-Y. Xu, W. Li, and Y.-Q. Wang, "Effects of vehicle running mode on rail potential and stray current in DC mass transit systems," *IEEE Transactions on Vehicular Technology*, vol. 62, no. 8, pp. 3569–3580, 2013.

[13] C. L. Pires, S. I. Nabeta, and J. R. Cardoso, "ICCG method applied to solve DC traction load flow including earthing models," *IET Electric Power Applications*, vol. 1, no. 2, pp. 193–198, 2007.

[14] A. Dolara, F. Foiadelli, and S. Leva, "Stray current effects mitigation in subway tunnels," *IEEE Transactions on Power Delivery*, vol. 27, no. 4, pp. 2304–2311, 2012.

[15] C. A. Charalambous, I. Cotton, and P. Aylott, "Modeling for preliminary stray current design assessments: the effect of crosstrack regeneration supply," *IEEE Transactions on Power Delivery*, vol. 28, no. 3, pp. 1899–1908, 2013.

[16] C. A. Charalambous and P. Aylott, "Dynamic stray current evaluations on cut-and-cover sections of DC metro systems," *IEEE Transactions on Vehicular Technology*, vol. 63, no. 8, pp. 3530–3538, 2014.

[17] A. Ogunsola, L. Sandrolini, and A. Mariscotti, "Evaluation of stray current from a DC-electrified railway with integrated electric-electromechanical modeling and traffic simulation," *IEEE Transactions on Industry Applications*, vol. 51, pp. 5431–5441, 2015.

[18] Y.-S. Tzeng and R.-N. Wu, "Electric network solutions of dc transit systems with inverting substations," *IEEE Transactions on Vehicular Technology*, vol. 47, no. 4, pp. 1405–1412, 1998.

[19] Y.-S. Tzeng, N. Chen, and R.-N. Wu, "Modes of operation in parallel-connected 12-pulse uncontrolled bridge rectifiers without an interphase transformer," *IEEE Transactions on Industrial Electronics*, vol. 44, no. 3, pp. 344–355, 1997.

[20] M. Wu, "Uniform chain circuit model for traction networks of electric railways," *Proceedings of the Csee*, vol. 30, no. 28, pp. 52–58, 2010.

[21] Y. Cai, M. R. Irving, and S. H. Case, "Compound matrix partitioning and modification for the solution of branched auto-transformer traction feeds," *IEE Proceedings—Electric Power Applications*, vol. 143, no. 3, pp. 251–257, 1996.